Measuring the spatial deformation of a liquid-crystal on silicon display with a self-interference effect

DAVID MARCO,[1] ASTICIO VARGAS,[2] MARÍA DEL MAR SÁNCHEZ-LÓPEZ,[1,3] AND IGNACIO MORENO[1,4,*]

[1]*Instituto de Bioingeniería, Universidad Miguel Hernández de Elche, 03202 Elche, Spain*
[2]*Departamento de Ciencias Físicas, Universidad de La Frontera, Temuco, Chile*
[3]*Departamento de Física Aplicada, Universidad Miguel Hernández de Elche, 03202 Elche, Spain*
[4]*Departamento de Ciencia de Materiales, Óptica y Tecnología Electrónica, Universidad Miguel Hernández de Elche, 03202 Elche, Spain*
**Corresponding author: dmarco@umh.es*

Received XX Month XXXX; revised XX Month, XXXX; accepted XX Month XXXX; posted XX Month XXXX (Doc. ID XXXXX); published XX Month XXXX

We present a simple technique to characterize the spatial non-uniformity of a liquid-crystal on silicon (LCOS) spatial light modulator (SLM). It is based on illuminating the display with a wavelength out of the operation range, so there is a significant reflection at the output surface. As a consequence, a Gires-Tournois interferometer is directly created, without any alignment requirement and insensitive to vibrations. The beam reflected at the output surface is the reference beam, while the beam reflected at the silicon backplane is modulated with the addressed gray level in order to quantitatively derive its deformation. We provide an experimental demonstration using a LCOS-SLM designed to operate in the near-infrared (NIR) range, but illuminated with visible light.

http://dx.doi.org/10.1364/OL.99.099999

SLMs have become a common opto-electronic device in many laboratories, where they are used to display programmable optical elements. Parallel-aligned LCOS devices are nowadays widely employed to display phase-only patterns [1]. They are reflective devices that modulate the phase of an input beam linearly polarized along the direction of the liquid-crystal (LC) director.

One of the major issues when operating with LCOS displays is the spatial non-uniformity, which causes an aberration that must be considered when the SLM is used as a phase-only diffractive element. In fact, some companies provide customers with a correcting mask that must be added to the designed hologram in order to compensate for this backplane aberration. In other cases, the users must perform their own characterization. For that goal, several standard interferometric techniques have been applied [2-7]. Other recent techniques used the LCOS device itself to create the reference and test beams by adding some linear and/or quadratic phase patterns [8,9].

In this paper we propose a different approach based on illuminating the SLM with a wavelength out of the operation range. In this situation, the antireflection (AR) coating reflects a significant portion of the input beam. Since the output part of the display has good flatness, we use this reflection as the reference beam. The light transmitted by the AR layer is then reflected at the LCOS backplane, thus being affected by the non-uniformities in this surface. Multiple reflections are then produced, as analyzed in detail in [10]. Here, instead, we are interested in making the most of this undesired effect as a tool to characterize the backplane non-uniformity. Because the beam that reached the backplane can be modulated by the LC layer, this modulation can be used to obtain different interferograms simply by changing the addressed gray level. The results here presented show how the LCOS backplane aberration can be quantitatively derived from these interference patterns. Then, we employ this information to design a phase mask to correct this aberration.

Figure 1(a) shows the experimental set-up. A Hamamatsu LCOS-SLM model X10468-08 is used, with 792×600 pixels and Δ=20 μm pixel spacing. Each pixel has 8-bit resolution, so it can take values in a grayscale from g=0 to 255. The nominal wavelength operation range is 1000–1500 nm. However, we use visible light from a He-Ne laser of 543 nm. This beam is spatially filtered and collimated, and polarized along the direction of the LC director. A non-polarizing beam splitter (NPBS) deviates the reflected beam. The light reflected by the SLM can be regarded as composed of two beams [10]. Because the device is operated with a wavelength far outside the designed range, the AR coating reflects an important fraction of the input intensity, which we measured about 30% for the 543 nm wavelength. This light is not modulated and can be used as a reference plane wave provided this reflecting layer has good flatness. Another fraction of the input beam enters the SLM and reaches the backplane, where it is reflected and acquires the aberration caused by its spatial deformation. The interference of

these beams is produced by the light reflected on the LCOS-SLM, as shown in Fig. 1(b) for different gray levels. We emphasize that such interferograms arise directly from the SLM itself. Thus, no alignment or external interferometer arrangement is required.

In order to verify the flatness of the AR coating, we measured the wavefront of a plane wave reflected at the display for a circular section at the center with a radius of about 3 mm. The light reflected at the AR coating was separated from the rest by addressing a linear grating to the SLM and its wavefront was measured with a Shack-Hartman sensor (Thorlabs WFS30-7AR/M). Figure 1(c) shows the measured wavefront fitted to the 15 first Zernike polynomials in the unit circle. The maximum deformation at the selected zone is less than 0.1λ, comparable to a flat mirror.

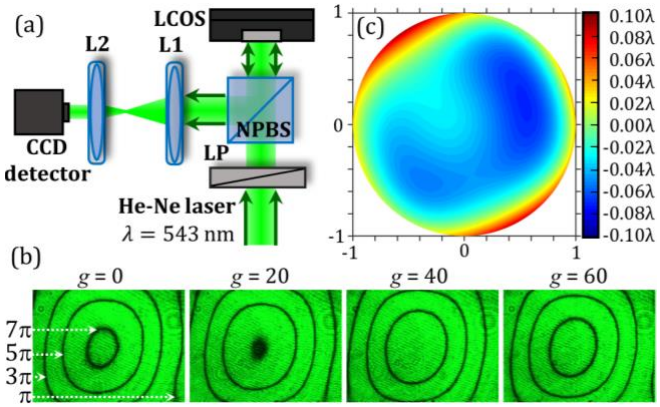

Fig. 1. (a) Scheme of the experimental set-up. LP: linear polarizer, NPBS: non-polarizing beam splitter, LCOS: Liquid crystal on silicon SLM, L1 and L2: Lenses. (b) Interference patterns obtained for different gray levels g. (c) Fit to the first 15 Zernike polynomials in the unit circle of the wavefront of the light reflected at the AR coating.

In the experiment in Fig. 1(a) the light reflected by the NPBS enters into a telescopic system (lenses L1 and L2) that forms the image of the SLM screen onto a CCD detector (Basler scA1390-17fc, with 1392×1040 pixels of 4.65×4.65 μm pixel size). We use this telescope to obtain an image of the LCOS-SLM screen instead of capturing a propagated interferogram, thus avoiding using back propagation algorithms. The focal lengths are f_1=25 cm and f_2=10 cm, in order to create an image with magnification M=-0.4, so that the complete image of the LCOS screen fits inside the CCD detector area. Figure 1(b) shows different interferograms captured when uniform images with g=0, 20, 40 and 60 are addressed to the SLM. Two important aspects must be considered: First, note that the dark fringes are very narrow compared to the bright areas. This is expected from a Gires-Tournois interferometer [11], where dark fringes are located only in a narrow area around the points where the phase difference between the reference and the test beams is an odd multiple of π. Secondly, note that there are four concentric fringes, indicating a backplane deformation from the center to the edges of the screen that causes more than 7π phase variation for this wavelength. When the gray level increases, these dark fringes move towards the center, as shown by the different interferograms in Fig. 1(b).

We consider that the light beam that enters the LCOS-SLM gains a phase ϕ_{Total} that is the sum of two terms: 1) the phase ϕ_{LC} that gains due to the double pass through the liquid-crystal (LC) layer, which is considered spatially uniform but depends on the gray level g, and 2) the phase caused by the backplane deformation ϕ_{BP}, which only depends on the spatial coordinates on the SLM, but not on g, i.e. $\phi_{Total}(g,x,y) = \phi_{LC}(g) + \phi_{BP}(x,y)$. The dark fringes move with the gray level because the phase $\phi_{LC}(g)$ changes with g. They appear where the phase ϕ_{Total} attained by the light inside the LCOS-SLM is an odd multiple of π, compared to the reference beam reflected at the AR coating. We verified for this device that the phase $\phi_{LC}(g)$ increases with g by using a spectral birefringence technique [12,13]. Because $\phi_{LC}(g)$ increases with g and the fringes move towards the center, we conclude that the phase ϕ_{BP} decrease towards the center, so the backplane is convex from the point of view of the laser source.

Since the interferograms obtained are not simply two-beam interference patterns (they are multiple-beam interferograms) they cannot be analyzed with a simple standard heterodyne technique. Instead, we apply a method based on the identification of the dark fringes. This information is used to obtain a correcting phase mask $\phi_C(x,y) = \phi_0 - \phi_{BP}(x,y)$, where ϕ_0 is a constant phase bias that can be adjusted. This correction can be implemented via a gray-scale spatial pattern $g_C(x,y)$ addressed to the SLM such that $\phi_{LC}[g_C(x,y)] = \phi_C(x,y)$. We arbitrarily choose $\phi_0 = 8\pi$ so the correcting mask has positive phase values in all pixels. Regarding the convex shape of the backplane, the correction phase function $\phi_C(x,y)$ must decrease from the center to the edges. The dark fringes in Fig 1(b), case g=0 are chosen as the reference for its calculation. We consider that the outer fringe in Fig. 1(b) g=0 corresponds to a phase ϕ_C of π, the next one is 3π, then 5π and finally the inner fringe is 7π, as indicated in the figure. In order to find the phase values in the rest of the screen, we track the position of the dark fringes in interferograms obtained for other values of g.

We identified that the fringe pattern for g=0 is repeated for g=80, meaning that the LC phase ϕ_{LC} increases by 2π. Since Hamamatsu provides SLMs with a linear phase response with g, we assume that it increases as $\phi_{LC}(g) = \phi_{LC}(0) + 2\pi g/80$, where $\phi_{LC}(0)$ is the minimum LC phase. Therefore, there is a phase difference of $\pi/2$ radians between the interference patterns shown in Fig 1(b) for g=0, 20, 40 and 60. For other gray levels in between, the dark fringes appear located at positions where the phase correction ϕ_C must be assigned with a phase function that adds $2\pi(g/80)$ to the value assigned to the same fringe when g=0.

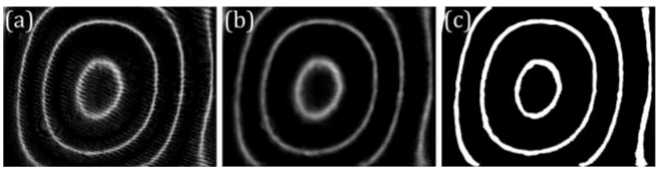

Fig. 2. Image processing procedure to precisely detect the dark fringes of the interferogram for g=0. (a) Gray level image resulting from subtracting the interferogram for g=0 to the interferogram for g=40. (b) Result after a median filter is applied to the image 2(a). (c) Result after binarization of the image 2(b).

In order to precisely localize the dark fringes of the interferograms we follow these steps: First, we remove some noise in the experimental images by subtracting each interferogram from another interferogram that is phase shifted by π (a gray level difference of 40) and set the negative values to zero. As a consequence, we obtain a gray level image as shown in Fig. 2(a),

which is obtained by subtracting the image in Fig. 1(b), g=0 from the image in Fig. 1(b), g=40. This operation cancels out the noise that is common in the two interferograms. Pixels that are bright in both interferograms result in almost zero value; pixels that are dark for g=40 but bright for g=0 result in a negative value, that we assign to zero; only those pixels that are dark for g=0 and bright for g=40 result in a significant positive value. This way we localize in Fig. 2(a) the dark fringes in Fig. 1(b), g=0. We then apply a median filter to remove the remaining noise, while keeping the sharpness of the fringes (Fig. 2(b)). Finally, we set all the points over a given threshold to 1 and below it to 0. As a result, we obtain binary images like Fig. 2(c) that detect the dark fringes in Fig. 1(b). Figure 2(c) reveals that the lines are thick, so we localize their central part. This procedure is applied to the interferograms in Fig. 1(b) and to other captured for gray levels in between (g=0, 20, 30, 48 and 66). As a result, we obtain a set of concentric lines corresponding to well identified points with the same phase. We use this information to determine the continuous 2D compensating phase function $\phi_C(x,y)$. The results are shown in Fig. 3.

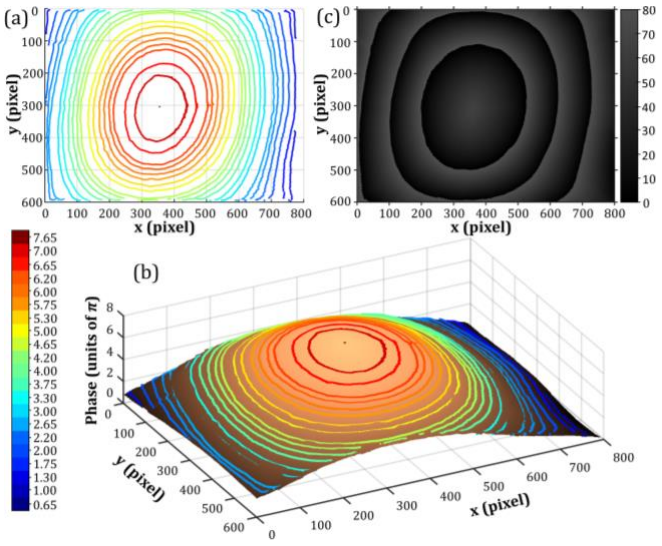

Fig. 3. Phase $\phi_C(x,y)$ that compensates the backplane deformation. (a) Scatter plot of the phase levels obtained from the dark fringes in interferograms for different gray levels. (b) Corresponding 3D plot of the fitted phase. The phase value for (a) and (b) is indicated in a color bar in units of π at the left of (b). (c) Gray level compensating mask.

Figure 3(a) presents a scatter plot of lines of equal phase and the corresponding fitted 3D map is represented in Fig. 3(b). This continuous function is obtained by applying a least-square polynomial fit to the data in Fig. 3(a) for each polar coordinate (in steps on one degree). The center of the polar coordinate system is located in the center of the aberration, which is determined as the central point of the inner fringe when it almost disappears (situation that occurs with g=26). Then, a phase value $7\pi + 2\pi g/80 = 7.65\pi$ is assigned to this central point. The polynomial fit is done in two different regions because the central part of the deformation has a greater curvature than the region at the edges, which is closer to be linear. The first region includes the phase values from 7.65π to 6.00π. We calculate the distance from the center of the aberration to every pixel and we apply a fit to the phase versus distance data. The same procedure was followed for the second region with data from 6.00π to 0.65π, but this time we use the distance from a point of the line of phase 6.00π to the other points. Combining the phase functions obtained for the two regions we get the phase $\phi_C(x,y)$ required at each point to compensate the deformation of the SLM screen. Figure 3(b) shows a 3D plot of this phase and the experimental lines that were used to determine it, also shown in Fig. 3(a). Finally, the gray-level mask that compensates the aberration is obtained. Each value of the phase function shown in Fig. 3(b) is assigned to a gray level by multiplying it by a factor of $80/2\pi$. However, this required phase correction has a phase variation (almost 8π) greater than the phase modulation in the gray level range from 0 to 255. Therefore, the phase values are then wrapped so they go from g=0 to 80 (phases from 0 to 2π), and finally the mask $g_C(x,y)$ shown in Fig. 3(c) is obtained. This mask must be added to any phase mask to compensate the SLM backplane deformation.

In order to verify the effectiveness of this correction mask, we perform two kinds of experiments. The first one consists simply in adding the correction and examine the interference pattern. We call this as the near-field corrected image, since we capture the image of the SLM plane, in the same set-up in Fig. 1. Figure 4(a1) shows again an image of the interferogram obtained for g=0, whereas Fig. 4(a2) shows the captured image when the correction mask in Fig. 3(c) is applied. Note how the interference fringes almost disappear, thus indicating an effective compensation of the aberration induced by the backplane deformation.

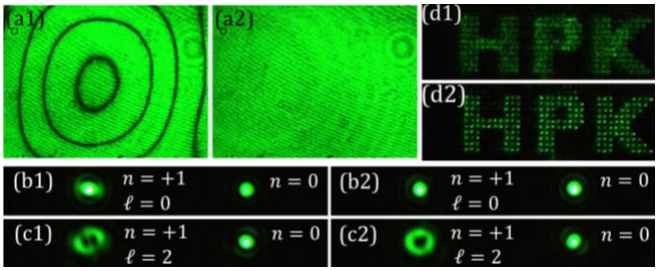

Fig. 4. Experimental results for 543 nm. (a) Near field interferograms without (a1) and with the correction (a2). (b,c) Far field results for forked blazed diffraction gratings without (b1, c1) and with correction (b2, c2). (b) Charge 0, (c) charge ℓ=2. (d) Reconstruction of a computer-generated hologram without (d1) and with correction (d2).

However, the correction shown in Fig. 4(a2) is not a complete demonstration of the effectiveness of the technique. In order to further verify this correction, we perform a second set of experiments where the far-field pattern generated with a phase diffractive element is analyzed. In this case, the telescopic system in Fig. 1(a) is replaced by a converging lens that forms the Fourier transform of the SLM screen onto the CCD detector. We start by choosing a blazed diffraction grating, and a blazed forked grating (Figs. 4(b)-(c)). Each subfigure shows the zero-diffraction order (right spot, n=0) and the first diffraction order (left spot, n=+1). The zero order is caused mainly by the non-modulated beam reflected at the SLM external surface and focuses on axis. Note how this beam appears well-focused in all cases, thus confirming the good flatness of this reflection. On the contrary, the first order appears clearly distorted in Fig. 4(b1), when no correction is applied, denoting the aberration this beam acquires when it is reflected by the LCOS backplane. It becomes well-focused when the correction mask is added (Fig. 4(b2)). Figures 4(c1) and 4(c2) show equivalent results

for a forked grating resulting from the combination of the blazed linear grating with a spiral phase of two cycles (ℓ=2). This grating generates a vortex beam in the first diffraction order. Vortex beams are very sensitive to aberrations and it is easy to identify when they are corrected since they produce focused spots in the form of a circular ring of light [14]. Note how the distortion in the vortex beam is significantly improved when we apply the correction mask, resulting in a focused spot with circular shape. Let us mention that in these results. we do not illuminate the complete SLM screen since we use a circular diaphragm before the SLM to get a circular input beam. This is necessary to better identify the circular shape of the focused diffraction orders.

Finally, Figs. 4(d1) and 4(d2) show the results when we display a Fourier transform computer generated hologram (CGH); in this case we illuminate the full SLM screen. Figure 4(d1) shows the reconstruction of the hologram without correction, and Fig. 4(d2) when the correction mask is applied. Note how the CGH reconstruction significantly improves and appears much better focused. A strong zero order (not shown) appears under the hologram reconstruction, again caused mainly by the reflection at the outer surface.

These results in Fig. 4 prove the correction at the same wavelength of 543 nm used for the characterization. Finally, we prove that this characterization of the SLM aberration can be extended to wavelengths within the operation range of the device. In Fig. 5 we show results of the CGH reconstruction for the wavelength of 1064 nm. In order to obtain an appropriate correction mask it is necessary to consider the dispersion of the LC layer. This can be done by measuring the spectral retardance using well-established techniques [12,13] where the SLM is placed between polarizers oriented at 45° to the LC director and it is illuminated with light of continuous broadband spectrum (we used a supercontinuum laser from FYLA, SC500 model).

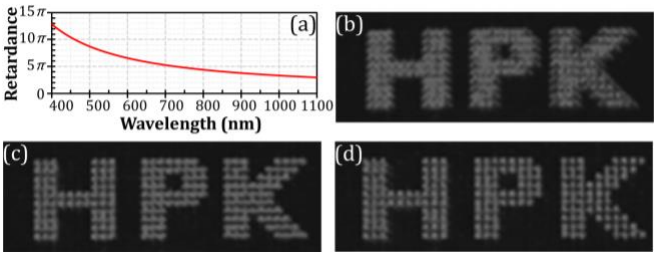

Fig. 5. (a) Spectral retardance measured for the LCOS device. Hologram reconstruction for 1064 nm (b) without correction (c) with our correction mask (d) with the mask provided by the manufacturer.

Figure 5(a) shows the measured spectral retardance, which shows a ratio of 2.48 between the value for λ=543 nm and for λ=1064 nm. A new correction mask for 1064 nm is obtained by rescaling the phase correction function in Fig. 3(b), wrapping it modulo 2π, and applying the gray level that corresponds to a phase modulation of 2π for 1064 nm (g=154 according to the manufacturer). The wavelength of 1064 nm is obtained placing a 1064 nm filter after the supercontinuum laser and the hologram reconstruction is captured with a camera from Raptor Photonics (Owl 640 Mini VIS-SWIR, with 640×512 pixels and 15 μm pixel pitch). The result without correction is presented in Fig. 5(b), which appears clearly defocused. Figures 5(c) and (d) show the corresponding result when we apply our correction mask and with the correction file that the manufacturer provides, respectively. Note how the results are very similar and notably improve the result without correction.

In summary, we present a novel and very simple method of determining the spatial deformation of a LCOS-SLM that does not require an external interferometric system. As a consequence, the experimental system is very stable under external conditions. The method is based on illuminating the device with a wavelength out of the operating range. In this situation, the outer AR coating partially reflects the incoming beam, and partially transmits light to the LC layer and reflects it at the backplane. Thus, reflected light from the SLM directly generates an interferogram that provides the information to infer the backplane spatial deformation. We show how the fringes shift by changing the addressed gray level, and this provides the information to derive phase-level maps that compensate this spatial deformation. We prove the effectiveness of this correction in the near field and in the far field, for the same wavelength of characterization, but also for a wavelength within the operation range.

Funding. Generalitat Valenciana, Conselleria d'Educació, Investigació, Cultura i Esport (PROMETEO-2017-154), Ministerio de Ciencia, Innovación y Universidades, Spain (RTI2018-097107-B-C33) and Fondo Nacional de Desarrollo Científico y Tecnológico ANID/FONDECYT 1191811, Chile.

Disclosures. The authors declare no conflicts of interest.

References

1. Z. Zhang, Z. You, and D. Chu, Light Sci. Appl. **3**(10), e213 (2014).
2. X. D. Xun and R. W. Cohn, Appl. Opt. **43**(35), 6400 (2004).
3. J. Oton, P. Ambs, M. S. Millán, and E. Pérez-Cabré, Appl. Opt. **46**(23), 5667 (2007).
4. D. Engström, M. Persson, J. Bengtsson, and M. Goksör, Opt. Express **21**(13), 16086 (2013).
5. T. Haist, C. Lingel, R. Adler, and W. Osten, Appl. Opt. **53**(7), 1413 (2014).
6. L. Teng, M. Pivnenko, Br. Robertson, R. Zhang, and D. Chu, Opt. Express **22**(21), 26392 (2014).
7. J. Xu, S. Qin, C. Liu, S. Fu, and D. Liu, Opt. Lett. **43**(12), 2993 (2018).
8. J. L. Martínez, E. J. Fernández, P. M. Prieto, and P. Artal, Opt. Express **24**(13), 14159 (2017).
9. H. Zhang, A. Lizana, C. Iemmi, F. A. Monroy-Ramírez, A. Márquez, I. Moreno, and J. Campos, Opt. Lasers Eng. **106**, 147 (2018).
10. J. L. Martínez, I. Moreno, M. M. Sánchez-López, A. Vargas, and P. García-Martínez, Opt. Express **22**(21), 25866 (2014).
11. P. Yeh, "Gires-Tournois interferometers", Section 7.2 in *Optical Waves in Layered Media*, 2nd Ed., John Wiley & Sons (2005), pp. 150-151.
12. A. Messaadi, M. M Sánchez-López, P. García-Martínez, A. Vargas, and I. Moreno, J. Eur. Opt. Soc. **12**(1), 1-9 (2016).
13. A. Vargas, M. M. Sánchez-López, P. García-Martínez, J. Arias, and I. Moreno, J. Appl. Phys. **115**(3), 033101 (2014).
14. A. Jesacher, A. Schwaighofer, S. Fürhapter, C. Maurer, S. Bernet, and M. Ritsch-Marte, Opt. Express **15**(9), 5801 (2007).

References

1. Z. Zhang, Z. You, and D. Chu, "Fundamentals of phase-only liquid crystal on silicon (LCoS) devices", Light Sci. Appl. **3**(10), e213 (2014).
2. X. D. Xun and R. W. Cohn, "Phase calibration of spatially nonuniform spatial light modulators," Appl. Opt. **43**(35), 6400–6406 (2004).
3. J. Oton, P. Ambs, M. S. Millán, and E. Pérez-Cabré, "Multipoint phase calibration for improved compensation of inherent wavefront distortion in parallel aligned liquid crystal on silicon displays," Appl. Opt. **46**(23), 5667–5679 (2007).
4. D. Engström, M. Persson, J. Bengtsson, and M. Goksör, "Calibration of spatial light modulators suffering from spatially varying phase response", Opt. Express **21**(13), 16086-16103 (2013).
5. T. Haist, C. Lingel, R. Adler, and W. Osten, "Parallelized genetic optimization of spatial light modulator addressing for diffractive applications", Appl. Opt. **53**(7), 1413-1418 (2014).
6. L. Teng, M. Pivnenko, Br. Robertson, R. Zhang, and D. Chu, "A compensation method for the full phase retardance nonuniformity in phase-only liquid crystal on silicon spatial light modulators", Opt. Express **22**(21), 26392-26402 (2014).
7. J. Xu, S. Qin, C. Liu, S. Fu, and D. Liu, "Precise calibration of spatial phase response nonuniformity arising in liquid crystal on silicon", Opt. Lett. **43**(12), 2993-2996 (2018).
8. J. L. Martínez, E. J. Fernández, P. M. Prieto, and P. Artal, "Interferometric method for phase calibration in liquid crystal spatial light modulator using a self-generated diffraction grating", Opt. Express **24**(13), 14159–14171 (2017).
9. H. Zhang, A. Lizana, C. Iemmi, F. A. Monroy-Ramírez, A. Márquez, I. Moreno, and J. Campos, "LCoS display phase self-calibration method based on diffractive lens schemes", Opt. Lasers Eng. **106**, 147–154 (2018).
10. J. L. Martínez, I. Moreno, M. M. Sánchez-López, A. Vargas, and P. García-Martínez, "Analysis of multiple internal reflections in a parallel aligned liquid crystal on silicon SLM", Opt. Express **22**(21), 25866-25879 (2014).
11. P. Yeh, "Gires-Tournois interferometers", Section 7.2 in *Optical Waves in Layered Media*, 2nd Ed., John Wiley & Sons (2005), pp. 150-151.
12. A. Messaadi, M. M Sánchez-López, P. García-Martínez, A. Vargas, and I. Moreno, "Optical system for measuring the spectral retardance function in an extended range," J. Eur. Opt. Soc. **12**(1), 1-9 (2016).
13. A. Vargas, M. M. Sánchez-López, P. García-Martínez, J. Arias, and I. Moreno, "Highly accurate spectral retardance characterization of a liquid crystal retarder including Fabry-Perot interference effects", J. Appl. Phys. **115**(3), 033101 (2014).
14. A. Jesacher, A. Schwaighofer, S. Fürhapter, C. Maurer, S. Bernet, and M. Ritsch-Marte, "Wavefront correction of spatial light modulators using an optical vortex image", Opt. Express **15**(9), 5801 (2007).